

A Novel Class of Endothelin-A Receptor Antagonists, (*R*)-2-(benzo[1,3]dioxol-5-yl)-6-isopropoxy-2*H*-chromene-3-carboxylic Acids (S-1255). Conformational Analysis of Basic Structure, Crucial for ET_A Antagonism, in Solution and Solid States

Natsuki Ishizuka,* Ken-ichi Matsumura, Junko Kikuchi and Hiroshi Nakai

Shionogi Research Laboratories, Shionogi & Co., Ltd., 12-4, Sagisu 5-chome, Fukushima-ku, Osaka 553-0002, Japan

Received 26 April 2002; accepted 8 July 2002

Abstract—Conformational studies of potent and selective endothelin-A (ET_A) receptor antagonists, 4-substituted (*R*)-2-(benzo[1,3]dioxol-5-yl)-6-isopropoxy-2*H*-chromene-3-carboxylic acids, are reported. X-ray crystallography and NMR studies of the 4-anisyl derivative **2** (S-1255), the stable atropisomers **3** and the 4-*n*-butyl derivative **4** reveal that the A-, B- and C-rings in these compounds adopt a L-like conformation in both solution and solid states. Molecular mechanics calculation shows that this L-like conformation is an inevitable conformation as determined by intramolecular steric repulsions. These 2*H*-chromene derivatives bound to an ET_A receptor with IC₅₀ values of less than 1 nM, whereas the dihydro compounds **7** and **9** not having the L-like conformation showed weaker affinities. These results suggest that the L-like conformation is specifically recognized by the active site of the ET_A receptor. The roles of the L-like conformation in the receptor binding are discussed.

© 2002 Elsevier Science Ltd. All rights reserved.

Introduction

Endothelins (ETs) are endogenous vasoconstrictive peptides with 21 amino acids¹ and have been implicated in various disease states.¹ Because of the promising therapeutic potential of ET_A receptor antagonists, a number of peptide and non-peptide ET_A receptor antagonists have been developed for treating various cardiovascular diseases.²

In a previous paper,³ we reported the discovery of (*R*)-2-(benzo[1,3]dioxol-5-yl)-6-isopropoxy-2*H*-chromene-3-carboxylic acids (**1**) as a novel class of ET_A receptor antagonists. In particular, the 4-anisyl derivative **2** (S-1255) was found to be a highly potent and orally active antagonist and was selected as a clinical candidate. Extensive chemical modifications during the course of development of **2** have revealed that the *m,p*-methylenedioxyphenyl, carboxyl and isopropoxy groups at the 2-, 3- and 6-positions, respectively, on the (*R*)-2*H*-chromene skeleton are essential for the potent ET_A antagonism and act as two hydrogen bonding acceptors and a

donor in the active site. Any substituent at the 4-position is acceptable provided its length is 6–9 Å. On the basis of these results, we have concluded that structure **1** is the basic structure crucial for specific recognition by the active site of the ET_A receptor (Fig. 1).

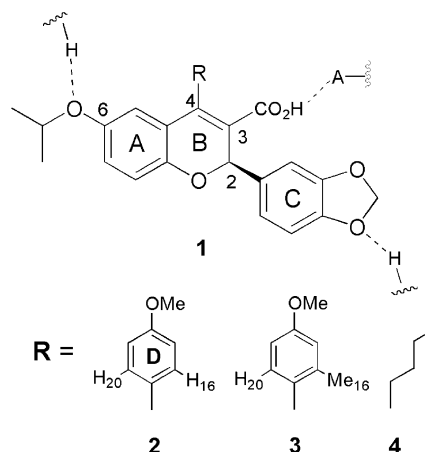


Figure 1. Speculated pharmacophore model of **1**. H- and A- indicate a hydrogen and a hydrogen bonding acceptor on the receptor active sites, respectively.

*Corresponding author. Tel.: +81-6-6458-5861; fax: +81-6-6458-0987; e-mail: natsuki.ishizuka@shionogi.co.jp

Because the ET_A receptor belongs to a class of the G protein-coupled receptors that are difficult to be purified and crystallized, the most realistic method to understand a three-dimensional ligand–receptor interaction is a conformational analysis of a free ligand.⁴ Having discovered the potent 2*H*-chromene antagonists, we have directed our attention to the study of the three-dimensional structure of **1**. In this paper, we will describe the conformational analysis of **1** in the solution and crystal states by NMR studies of **2**, the stable atropisomers **3** and the 4-*n*-butyl analogue **4** as well as by X-ray crystallography of **2** and **4**. These compounds are potent and selective ET_A receptor antagonists having the optimized substituents at the 2-, 3- and 6-positions and different substituents only at the 4-position (Fig. 1). The roles of the three-dimensional structures affecting the binding affinity are also discussed on the basis of the experimental results.

Results and Discussion

Synthesis

Synthesis of all compounds except for the Me16 derivative **3** has been described in the previous paper.³ Synthesis of **3** is shown in Figure 2. The enantiomerically pure 4-methoxy acid **5**³ was treated with 4-methoxy-2-methylphenyl magnesium bromide in THF to give **3** as a 2:5 mixture of diastereomeric atropisomers around the C4–C15 axis as determined by ¹H NMR. After being equilibrated in refluxing methanol, the mixture was separated into its atropisomeric counterparts by preparative reversed-phase HPLC.

The absolute configurations of the atropisomers around the C4–C15 axis were determined by NOE experiments. NOE cross-peaks were observed between the H20 proton and the H10 and H14 protons in the polar isomer and between the Me16 protons and the H10 and H14

protons in the less polar isomer (Fig. 2). The relative configurations between the Me16 and the C-ring were therefore determined to be *anti* for the former and *syn* for the latter. Because the absolute *R*-configuration of the 2-position in **5** had been established,³ the absolute configurations of the polar and less polar isomers can be assigned as *R,aS* and *R,aR*, respectively, as shown in Figure 2. In the following discussion, (*R,aS*)- and (*R,aR*)-atropisomers are referred to *anti*-**3** and *syn*-**3**, respectively, for convenience. Diastereomeric and enantiomeric excess of *anti*-**3** and *syn*-**3** were 96% de and 97% ee, and 92% de and 99% ee, respectively, as determined by the HPLC methods.

Unless otherwise stated, all the structures described in this paper indicate the absolute configurations. The four rings are referred to the A-, B-, C- and D-rings as shown in Figure 1.

X-ray crystallography

X-ray crystallography of the 4-*p*-anisyl compound **2** and the 4-*n*-butyl compound **4** was carried out. Two independent molecular structures were included in each crystal. These molecules were treated independently, being called M1 and M2 for **2** and M3 and M4 for **4**, respectively, in the following discussion.

Representative views of the space-filling models of M1 and M3 are illustrated in Figures 3A and 4A, respectively. The crystal structures of M2 and M4 are essentially identical to those of M1 and M3, respectively, except for the geometry of the 3-carboxyl and 6-isopropoxy groups.

The selected torsion angles are tabulated in Table 1. Regardless of the difference in the 4-substituent, the conformations of the A-, B- and C-rings are essentially identical among the four crystal structures. The averaged torsion angles of O1–C4b–C4a–C5, C2–C1–C4b–C4a,

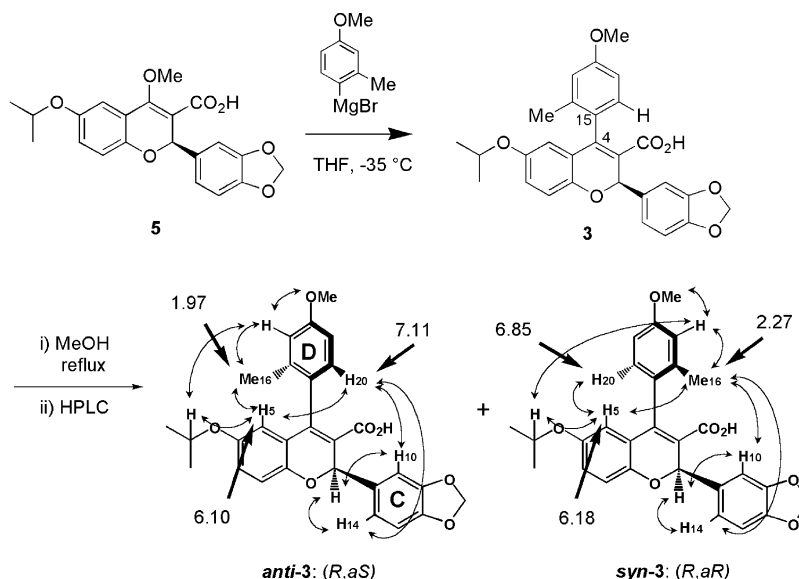


Figure 2. Synthetic scheme of and NOE correlations and chemical shifts (δ) of H5, Me16 and H20 in *anti*-**3** and *syn*-**3**. Observed NOE correlations are represented by double-headed arrows. Irrelevant hydrogens are omitted for clarity.

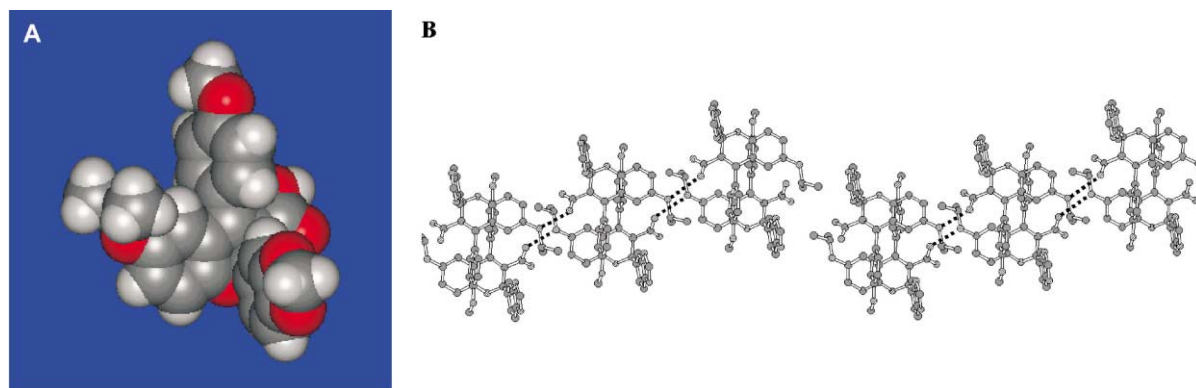


Figure 3. A: A space-filling model of the X-ray crystal structure of **2** (M1). Gray, red and white indicate the carbon, oxygen and hydrogen atoms, respectively. B: A stereoview of part of the packing structure of **2**. All hydrogens are omitted for clarity. The anisyl group in **2** is fitted into the L-like region consisting of the A-, B- and C-rings in a nearby molecule, forming an aromatic edge-to-face interaction. The intermolecular hydrogen bonds represented by the dotted lines are observed between the carboxyl hydrogen and the isopropoxy oxygen.

C3–C4–C4a–C4b, C3–C2–O1–C4b and C4–C4a–C5–C6 are 176, 32, –13, –46 and 176°, respectively (Table 1), indicating that the A/B-ring portion is almost coplanar except for the C2 atom that is positioned 0.5 Å above the mean plane of the A- and B-rings. Thus, the B-ring adopts a C2 envelope conformation.

Each C-ring stands almost upright above the mean plane of the A- and B-rings, as indicated by the averaged torsion angle of C4–C3–C2–C9 to be nearly 90°. The small torsion angle (4–12°) of C3–C2–C9–C10 indicates that the plane of the C-ring faces toward the A-ring. Consequently, the overall shape consisting of the A-, B- and C-rings looks like a capital 'L', forming a hydrophobic pocket around the orthogonal corner in this L-like wall, as shown in Figures 3A and 4A. In the following discussion, this region is referred to the L-like region. This conformational feature is essentially common to all the related crystal structures (data not shown).⁵

Table 1. Selected torsion angles (°) for the crystal structures of **2** (M1 and M2) and **4** (M3 and M4)

	M1	M2	M3	M4	Mean
O1–C4b–C4a–C5	173.6	177.9	175.5	175.9	175.7
C2–C1–C4b–C4a	29.8	28.8	31.0	36.4	31.5
C3–C4–C4a–C4b	–9.1	–12.9	–13.3	–16.8	–13.0
C3–C2–O1–C4b	–41.0	–48.5	–45.4	–49.8	–46.2
C4–C4a–C5–C6	177.4	172.4	175.4	179.0	176.1
C4–C3–C2–C9	–96.3	–85.3	–92.2	–93.2	–91.8
C3–C2–C9–C10	12.1	4.8	175.7	–179.1	—
C3–C4–C15–C16	77.0	115.7	—	—	96.4 ^a
C2–C3–C21–O22	47.1	–15.4	–147.4	–170.9	—
C5–C6–C23–C24	25.1	–8.2	–179.9	167.4	—

^aMean of M1 and M2.

The D-ring in **2** is almost perpendicular relative to the B-ring. The space-filling model (Fig. 3A) clearly shows that this orthogonal conformation of the D-ring results from the steric hindrance of the *peri*-hydrogen at the 5-position (H5). The *n*-butyl group in **4** adopts an extended staggered conformation (Fig. 4A).

The noteworthy intermolecular interactions observed in the packing diagrams are shown in Figures 3B and 4B. In the packing structure of **2** (Fig. 3B), the D-ring of one molecule is fitted into the L-like region of another nearby molecule. The angle between the D-ring and the paired A-ring is 72–96° and the distance between these two centroids is 5.1–5.3 Å, indicating the formation of the aromatic edge-to-face interaction.⁶ Similarly, the extended 4-*n*-butyl group in **4** is fitted into the L-like region of another nearby molecule, forming a tight hydrophobic interaction (Fig. 4B).

Intermolecular hydrogen bonds are formed between the 3-carboxyl hydrogen as a donor and the 6-isopropoxy oxygen as an acceptor in the packing structure of **2**, forming head-to-tail hydrogen bonding networks (Fig. 3B). In contrast, the carboxyl groups in **4** form a carboxylic acid dimer structure (Fig. 4B).

NMR studies

Determination of the D-ring geometry. In order to know the conformation of **1** in solution, NMR studies were carried out first on **2** and **4**. The spectra were recorded in CDCl₃ at a range of –15 to 60 °C at 600 MHz.

In ¹H NMR spectrum of **2**, the two *o*-protons on the D-ring, H16 and H20, appear as a very broad single signal at 25 °C (Fig. 5). The broadening is still visible even at 60 °C. This broad signal begins to separate at 10 °C, and two broad signals with an AB-pattern appear at –15 °C. This temperature effect is also reflected in ¹³C NMR of **2**. Thus, the corresponding *o*-carbons, C16 and C20, were observed as a single peak at 130.2 ppm at 25 °C and as two separate peaks at 129.7 and 130.4 ppm below 10 °C.

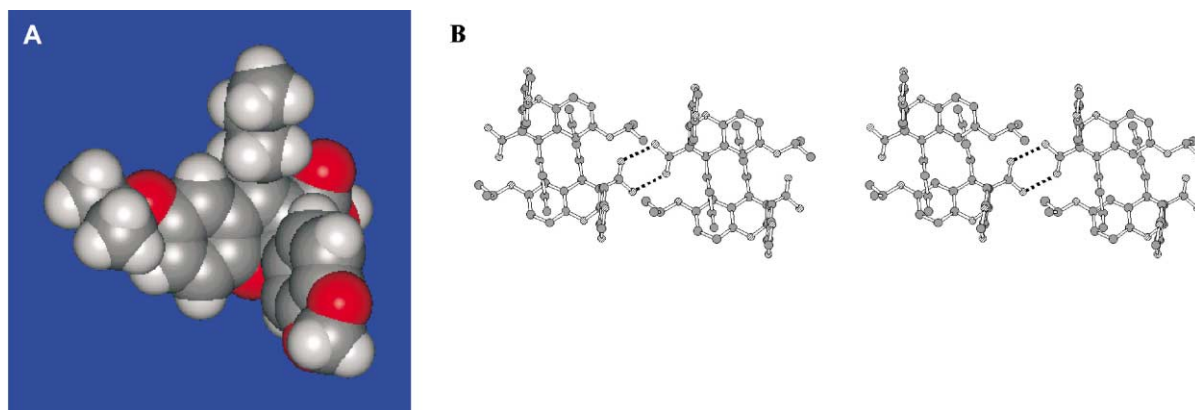


Figure 4. (A) A space-filling model of the X-ray crystal structure of **4** (M3). Gray, red and white indicate the carbon, oxygen and hydrogen atoms, respectively. (B) A stereoview of part of the packing structure of **4**. All hydrogens are omitted for clarity. The *n*-butyl group in **4** is fitted into the L-like region consisting of the A-, B- and C-rings in a nearby molecule, forming a hydrophobic interaction. The intermolecular hydrogen bonds represented by the dotted lines are observed between the two carboxyl groups, forming the dimer structure.

The H5 signal in **2** was observed consistently around 6.2 ppm at all temperatures. This position is abnormally higher than that expected for this kind of aromatic proton. Indeed, the chemical shift of the H5 signal in **2** is 0.7 ppm higher than that of 4-*n*-butyl analogue **4** (Fig. 5A), suggesting that the H5 in **2** is in the shielding cone of the D-ring.

All these results strongly indicate that the free rotation of the D-ring in **2** is severely hindered by steric repulsion from the H5 proton, resulting in a broad signal of the D-ring *o*-protons above 10 °C, and that at –15 °C the D-ring is no longer able to rotate and gives two independent signals. The unusual upfield shift of the H5 evidently arises from the shielding effect of the D-ring, accounting for the perpendicular relationship between the D-ring and the A/B-rings. This predicted conformation of the D-ring in **2** in solution agrees with the conformation observed by its X-ray crystallography (Fig. 3A).

A similar signal broadening of the two *o*-protons and an upfield shift of the H5 proton were observed in all 4-phenyl substituted analogues of **2**. The data are tabulated in our previous paper.³ Thus, the A/B- and D-rings are consistently perpendicular in this type of compounds.

Determination of the C-ring geometry. The large difference in the chemical shifts between the two *o*-protons on the D-ring at –15 °C ($\Delta\delta = 0.22$, Fig. 5) suggests that these *o*-protons lie in magnetically different environments. Due to the limited rotation and perpendicular orientation of the D-ring, one of these *o*-protons is in the same side of the C-ring and the other is in the opposite side. Because these protons are positioned equivalently to the A/B-rings as well as to the 3- and 6-substituents, but not to the C-ring, only the ring current effect of the C-ring is responsible for this large difference in the chemical shifts.

Figure 6 shows the schematic representation of two possible anisotropic effects induced by the axial C-ring.⁷ When the plane of the C-ring faces toward the A-ring

(Fig. 6A), the *o*-proton closer to the C-ring (*X* = H) will suffer from the deshielding effect of the C-ring, being shifted to a lower field than the other (*Y* = H). When the plane of the C-ring faces toward the D-ring (Fig. 6B), on the other hand, the anisotropic effect of the C-ring will be reversed and the low-high relationship of these chemical shifts will be also reversed. This reversal relationship predicts that if *X* and *Y* are the different groups that are spectroscopically distinguishable, the C-ring geometry in solution can be determined by comparison of their chemical shifts.

To support this prediction, the methyl group (Me16) was introduced into the *o*-position of the D-ring (Fig. 2). As described in the Synthesis section, Grignard reaction of **5** afforded a mixture of the atropisomers around the C4–C15 axis, *anti*-**3** and *syn*-**3**. These isomers are stable at room temperature and readily separated by preparative reversed-phase HPLC. The signals at their two *o*-positions,

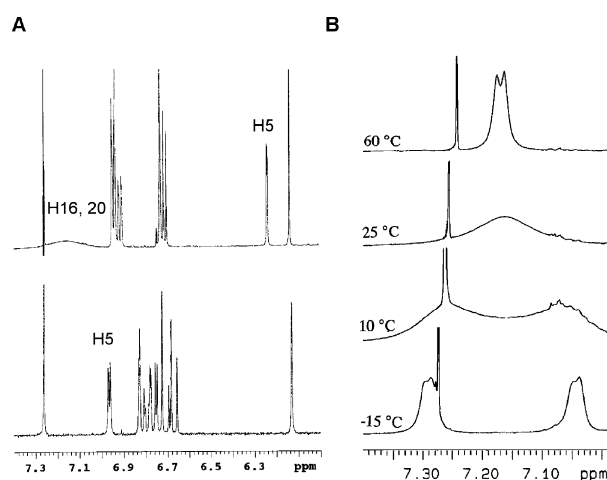


Figure 5. (A) Aromatic region in ¹H NMR spectra of **2** (top) and **4** (bottom) in CDCl₃ at 25 °C. The signals of the D-ring *o*-protons (H16 and H20) in **2** are broad and not separated. The H5 signal in **2** appears at 6.2 ppm, which is shifted to a higher field by about 0.7 ppm than that of **4**. (B) Temperature dependence of the D-ring *o*-proton signals in **2**. Two separate signals appear at –15 °C, which coalesce at 10 °C and become broad above 25 °C.

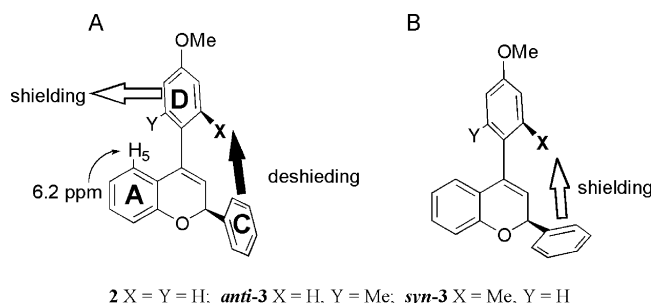


Figure 6. Two possible anisotropic effects induced by the C- and D-rings. The open arrow indicates the shielding effect and the solid arrow indicates the deshielding effect. The substituents at the 3- and 6-positions are omitted for clarity. (A) The plane of the C-ring faces toward the A-ring, giving the deshielding effect on X. (B) The plane of the C-ring faces toward the D-ring, giving the shielding effect on X.

X and Y, could be easily discriminated by a conventional NMR technique because the D-rings in both isomers does not rotate at room temperature.

^1H NMR spectra of *anti*-3 and *syn*-3 at 25 °C were essentially similar except for the Me16 and H20 signals. The H5 protons in both isomers were observed at about 6.1 ppm owing to the shielding effect of the D-ring, again demonstrating the perpendicularly orientated D-ring relative to the A/B-rings. The NOE cross-peaks observed between the D-ring *o*-protons and the C-ring *o*-protons (Fig. 2) indicate that the C- and D-rings are in close proximity (within 0.5 Å). Thus, an axial orientation of the C-ring in solution was unambiguously determined. This result agrees well with that of our CD spectrum study.⁷

In order to determine the orientation of the plane of the C-ring, ^1H NMR chemical shifts of the Me16 and H20 protons were compared between the two isomers. The Me16 protons in *syn*-3 (X = Me, 2.27 ppm) were shifted to a lower field by 0.3 ppm than those in *anti*-3 (Y = Me, 1.97 ppm). On the other hand, the H20 proton in *syn*-3 (Y = H, 6.85 ppm) was shifted to a higher field than that in *anti*-3 (X = H, 7.11 ppm). This low-high relationship of the chemical shifts can be explained only by the deshielding effect of the C-ring on the D-ring, as shown in Figure 6A, elucidating that the plane of the C-ring faces toward the A-ring but not toward the D-ring. The C-rings in **2** and its analogues are self-evidently determined to have conformations similar to those of *anti*-3 and *syn*-3. Therefore, the A-, B- and C-rings in the basic structure **1** was elucidated to adopt the L-like conformation in solution. This result is in good agreement with that from the above X-ray crystallography.

Molecular mechanics calculation

The characteristic L-like conformation of the A-, B- and C-rings in **2** and its analogues can be explained by a molecular model study and a molecular mechanics calculation. The molecular model study shows that the equatorial conformation of the C-ring is energetically unfavorable because of a severe allylic repulsion⁸ between the C-ring and the adjacent carboxyl group at the 3-position. This steric repulsion must push the C-ring away to the axial position with taking the C2 envelope conformation.

The molecular mechanics calculation⁹ of a simplified model compound of **2** predicts that the plane of the C-ring prefers to face toward the A-ring (Fig. 7), probably due to the van der Waals repulsion between the A- and C-rings as well as between the 3-carboxyl group and the C-ring. Thus the L-like conformation is elucidated to be stable and rigid.

Biological testing and structure–activity relationships

The binding affinities of **2** and its related compounds to the ET_A receptor were determined by their ability to competitively displace [¹²⁵I]ET-1 from its specific binding site.¹⁰ The affinities are expressed as IC₅₀ values and summarized in Table 2. The 2*H*-chromenes **2**, *anti*-3, *syn*-3 and **4** exhibited potent binding affinity with IC₅₀ values of less than 1 nM.

Previously, we showed that reduction of the C3–C4 double bond to give the dihydro compounds **7** and **9** resulted in decreasing the binding affinity³ (**6** vs **7** and **8** vs **9**, Table 2). The C-ring in the dihydro derivatives adopts the equatorial configuration,³ and thus they can no longer have the L-like conformation. This result indicates that the L-like conformation is specifically recognized by the active site of the ET_A receptor. Presumably, the L-like conformation plays a role in arranging the 2-, 3-, 4- and 6-substituents on the

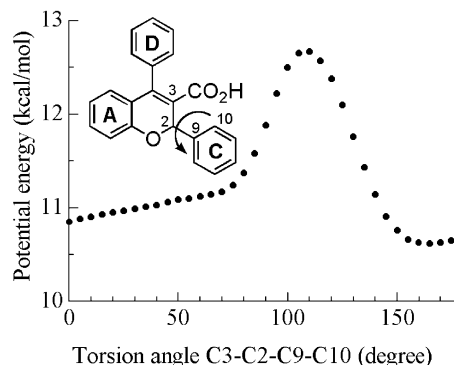
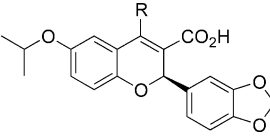
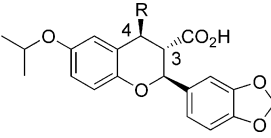
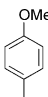
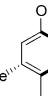
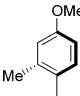
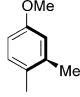


Figure 7. Conformational energy profile (kcal/mol) as a function of the C3–C2–C9–C10 torsion angle in the simplified compound of **2**, obtained from a grid search scan with an incensement of 5° (Tripos force field). The conformer in which the C-ring plane faces toward the A-ring (angle: about 170°) is more stable than the conformer in which the C-ring plane faces toward the D-ring (angle: about 110°).

Table 2. ET_A receptor binding affinity

Compd	R	ET _A ^a : IC ₅₀ (nM) ^b
<div style="display: flex; justify-content: space-around; align-items: center;"> <div style="text-align: center;">  <p>2, 3, 4 (<i>R</i>) 6, 8 (<i>RS</i>)</p> </div> <div style="text-align: center;">  <p>7, 9 (<i>RS</i>)</p> </div> </div>		
2		0.19 ± 0.01 (2) ^c
6	<i>n</i> -C ₄ H ₉	0.51 ± 0.04 (2) ^c
7		1.3 (1) ^c
4		0.42 ± 0.12 (2) ^c
8		0.73 ± 0.03 (2) ^c
9		77 ± 7 (2) ^c
<i>anti</i> -3		0.20 (1)
<i>syn</i> -3		0.91 (1)

^aRat receptors.^bA mean IC₅₀ values ± standard error with the number of experiments given in parentheses.^cCited from ref 3.

2*H*-chromene ring at the desired positions and directions of the receptor active sites. Consequently, our antagonists should be able to form preferable interactions with the ET_A receptor active site.

The data in Table 2 also suggest another role of the L-like conformation. Interestingly, **2** and *anti*-**3** exhibit similar binding affinities, whereas *syn*-**3** is 5 times less potent. The most plausible explanation of this difference is that the Me16 in *syn*-**3** occupying the upper part of the L-like region hinders the receptor binding. The L-like region acts as a hydrophobic pocket and accommodates the *p*-anisyl or *n*-butyl group in the crystal packing structure (Figures 3B and 4B). These observations suggest a possibility that the L-like region forms an edge-to-face or a hydrophobic interaction with the receptor.

Conclusion

The present study revealed the three-dimensional structure of our ET_A receptor antagonists having the 2*H*-chromene skeleton, including S-1255 (**2**). In both solid and solution states, the C-ring adopts the axial orientation and its plane faces toward the A-ring. Consequently, the A-, B- and C-rings in the basic structure **1** consistently adopt the L-like conformation. Inspection of the molecular models together with the molecular mechanics calculation reveals that this characteristic conformation is inevitably determined by the intramolecular

steric constraints. The ET_A receptor binding studies indicate that this L-like conformation plays crucial roles in the receptor recognition. The three-dimensional structure elucidated herein should be useful not only for gaining a deeper understanding of the mode of binding the antagonists to the ET_A receptor but also for designing novel and more potent ET_A receptor antagonists.

Experimental

General

¹H and ¹³C NMR spectra of **2**, **3**, and **4** were recorded on Varian Unity-600 instrument with trimethylsilane as an internal standard and the signals were fully assigned. Analytical and preparative HPLC were conducted on Shimadzu LC-10AD and Waters 6000A instruments, respectively. Column chromatography was performed using a column packed with Merck silica gel 60 (70–230 mesh). Synthesis of compounds **2** and **4–9** has been described in the preceding paper.³ The molecular mechanics calculation was performed on a Silicon Graphics Indigo R4400 workstation with the molecular modeling software package SYBYL 6.01.

(*R,aS*)- and (*R,aR*)-2-(Benzo[1,3]dioxol-5-yl)-6-isopropoxy-4-(4-methoxy-2-methylphenyl)-2*H*-chromene-3-carboxylic acids (*anti*-3** and *syn*-**3**).** A THF (7 mL) solution of 4-methoxy-2-methylphenyl magnesium bromide, prepared from 4-bromo-3-methylanisole (2.09 g, 10.4 mmol) and magnesium turnings (265 mg, 10.9 mmol) by a conventional procedure, was added dropwise to (*R*)-2-(benzo[1,3]dioxol-5-yl)-6-isopropoxy-4-methoxy-2*H*-chromene-3-carboxylic acid **5**³ (1.00 g, 2.60 mmol) in THF (6.5 mL) at –35 °C. After being stirred for 0.5 h at –35 °C and then 0 °C for 3 h, the reaction mixture was quenched with 1 M HCl (11.4 mL) and extracted with ethyl acetate. The extract was washed with water and brine, dried with MgSO₄ and then concentrated. The residue was purified by column chromatography on silica gel (ethyl acetate/hexane, gradient from 1/4 to 1/2), followed by recrystallization from acetone/isopropyl ether to give **3** (497 mg, 40%) as a 2:5 mixture of atropisomers *anti*-**3** and *syn*-**3**, as determined by ¹H NMR. The mixture was heated at reflux in methanol for 4 h to give a 1:1 equilibrated mixture.

Separation and purity determination of the atropisomers were carried out by HPLC under the following conditions: column, COSMOSIL 5C18AR (20×250 mm, Daicel Chemical); solvent, methanol/H₂O/trifluoroacetic acid=80/20/0.1; flow rate, 12 mL/min; detection, UV 285 nm. Enantiomeric purity was determined under the following conditions: column, CHIRALPAK AD (4.6×250 mm, Daicel Chemical); solvent, hexane/isopropanol/trifluoroacetic acid=90/10/0.1; flow rate, 0.5 mL/min; detection, UV 285 nm. *Anti*-**3**: a yellow oil. 96% de (*t*_R=21.7 min); 97% ee (*t*_R=20.5 min, (*S,aR*)-isomer: *t*_R=32.9 min). [α]_D²⁵+158.3 (c 0.477, CH₃OH). ¹H NMR (CDCl₃): δ 1.13 (3H, d, *J*=6.1 Hz), 1.17 (3H, d, *J*=6.1 Hz), 1.97

(3H, s), 3.86 (3H, s), 4.16 (1H, septet, $J=6.1$ Hz), 5.91 (2H, s), 6.13 (1H, d, $J=2.7$ Hz), 6.18 (1H, s), 6.72–6.95 (7H, m), 7.11 (1H, d, $J=8.0$ Hz). ^{13}C NMR (CDCl_3): δ 19.8, 21.7, 22.0, 55.4, 70.5, 74.4, 101.1, 108.1, 108.1, 111.0, 115.3, 115.7, 117.8, 120.1, 120.8, 121.3, 124.1, 128.1, 129.6, 132.7, 137.0, 147.2, 147.3, 147.7, 152.2, 159.4, 169.0. Anal. calcd for $\text{C}_{28}\text{H}_{26}\text{O}_7 \cdot 0.2\text{H}_2\text{O}$: C, 70.34; H, 5.57. Found: C, 70.08; H, 5.29. **Syn-3**: a yellow oil. 92% de ($t_{\text{R}}=22.9$ min); 99% ee ($t_{\text{R}}=26.8$ min, (*S,S*)-isomer: $t_{\text{R}}=23.0$ min). $[\alpha]_{\text{D}}^{25}+77.8$ (c 0.478, CH_3OH). ^1H NMR (CDCl_3): δ 1.15 (3H, d, $J=6.1$ Hz), 1.18 (3H, d, $J=6.1$ Hz), 2.27 (3H, s), 3.85 (3H, s), 4.18 (1H, septet, $J=6.1$ Hz), 5.91 (2H, s), 6.10 (1H, d, $J=2.7$ Hz), 6.25 (1H, s), 6.71–6.97 (8H, m). ^{13}C NMR (CDCl_3): δ 20.32, 21.8, 21.8, 55.4, 70.5, 75.0, 101.1, 108.0, 108.1, 111.3, 115.4, 115.7, 117.6, 119.7, 121.9, 122.0, 124.0, 128.4, 128.9, 133.1, 137.4, 146.2, 147.3, 147.7, 152.2, 159.2, 169.2. Anal. calcd for $\text{C}_{28}\text{H}_{26}\text{O}_7 \cdot 0.2\text{H}_2\text{O}$: C, 70.34; H, 5.57. Found: C, 70.05; H, 5.36.

Single-crystal X-ray analysis. X-ray diffraction measurements were performed at 295 K on a Rigaku AFC7R diffractometer using a graphite-monochromated $\text{Cu-K}\alpha$ radiation ($\lambda=1.54178$ Å) and a rotating anode generator. The data were corrected for Lorentz and polarization effects. The structure was solved by direct methods¹¹ and expanded using Fourier techniques. All calculations were performed using the teXsan¹² crystallographic software package of Molecular Structure Corporation. Crystallographic data for the structures in this paper have been deposited with the Cambridge Crystallographic Data Centre as supplementary publication nos. CCDC187972 for **2**; CCDC187973 for **4**. Copies of the data can be obtained, free of charge, on application to CCDC, 12 Union Road, Cambridge, CB2 1EZ, UK [fax: +44-(0)1223-336033 or e-mail: deposit@ccdc.cam.ac.uk].

2 (M1 and M2). Yellow prismatic crystals of **2**, $\text{C}_{27}\text{H}_{24}\text{O}_7$, were grown from a methanol solution. A single crystal with approximate dimensions, $0.30 \times 0.10 \times 0.05$ mm, was picked up and used for the X-ray data collection. Cell constants were obtained by the least-squares refinement using the setting angles of $45^\circ < 2\theta < 50^\circ$. Crystal data are as follows: space group $P2_1$; $a=10.358(3)$ Å, $b=9.926(2)$ Å, $c=22.115(3)$ Å, $\beta=91.37(2)^\circ$, $V=2273.0(9)$ Å³, $Z=4$, $D_{\text{cal}}=1.345$ g/cm³. Of the 4806 reflections which were collected ($2\theta \leq 140.2^\circ$), 4553 were unique, $\omega/2\theta$ mode with ω scan width was $(1.68+0.30 \tan\theta)^\circ$ and ω scan speed was $16.0^\circ/\text{min}$. The linear absorption coefficient, μ , for the $\text{Cu-K}\alpha$ radiation was 8.1 cm^{-1} . The non-hydrogen atoms were refined anisotropically. Hydrogen atoms in the OH group were refined isotropically, while the rest were included in fixed positions. The final cycle of the full-matrix least-squares refinement was based on 3426 observed reflections [$I > 2\sigma(I)$] and 621 variable parameters. Final R and weighted R values were 0.040 and 0.057, respectively. The maximum and minimum peaks on the final difference Fourier map corresponded to 0.13 and $-0.14 \text{ e}/\text{\AA}^3$, respectively.

4 (M3 and M4). Colorless prismatic crystals of **4**, $\text{C}_{24}\text{H}_{26}\text{O}_6$, were grown from a methanol solution. A single crystal with approximate dimensions, $0.10 \times 0.20 \times 0.35$ mm, was picked up and used for the X-ray data collection. Cell constants were obtained by the least-squares refinement using the setting angles of $45^\circ < 2\theta < 50^\circ$. Crystal data are as follows: space group $P1$; $a=11.1527(8)$ Å, $b=12.6592(7)$ Å, $c=8.891(1)$ Å, $\alpha=110.166(7)^\circ$, $\beta=104.685(7)^\circ$, $\gamma=97.417(5)^\circ$, $V=1106.9(2)$ Å³, $Z=2$, $D_{\text{cal}}=1.231$ g/cm³. Of the 4544 reflections which were collected ($2\theta \leq 140.2^\circ$), 4155 were unique, $\omega/2\theta$ mode with ω scan width was $(1.84+0.30 \tan\theta)^\circ$ and ω scan speed was $16.0^\circ/\text{min}$. The linear absorption coefficient, μ , for the $\text{Cu-K}\alpha$ radiation was 7.2 cm^{-1} . The non-hydrogen atoms were refined anisotropically. Hydrogen atoms in the OH group were refined isotropically, while the rest were included in fixed positions. The final cycle of the full-matrix least-squares refinement was based on 3656 observed reflections [$I > 2\sigma(I)$] and 548 variable parameters. Final R and weighted R values were 0.041 and 0.068, respectively. The maximum and minimum peaks on the final difference Fourier map corresponded to 0.22 and $-0.15 \text{ e}/\text{\AA}^3$, respectively.

ET_A receptors binding assay.¹⁰ The rat aorta smooth muscular cells were cultured on 48-well culture plates. After 3–5 days, the cluster medium was aspirated, and the cells were washed twice with an ice-cold HEPES-buffered Hank's solution (20 mM, pH 7.4). The cells in each well were incubated with 12.5 pM [¹²⁵I]ET-1 in the HEPES-buffered Hank's solution (0.3 mL) containing PMSF (0.1 mM), protinin (10 µg/mL), leupeptin (10 µg/mL), pepstatin A (10 µg/mL), bacitracin (250 µg/mL) and soybean trypsin inhibitor (10 µg/mL) in the absence or presence of a test compound at varying concentrations. Equilibrium binding studies were performed at 37°C for 60 min. The incubation was terminated by rapid removal of the incubation medium and addition of the ice-cold HEPES-buffered Hank's solution (0.25 mL). The free ligand was removed by washing the intact-attached cells two times with the ice-cold HEPES-buffered Hank's solution. The cells were dissolved in 0.1 M NaOH and transferred to a test tube, and then the radioactivity was counted. The nonspecific binding was determined in the presence of 10^{-7} M ET-1 and was about 5–10% of the total binding.

Acknowledgements

The authors are grateful to Dr. T. Shiota for the molecular mechanics calculation.

References and Notes

1. Yanagisawa, M.; Kurihara, H.; Kimura, S.; Tomobe, Y.; Kobayashi, M.; Mitsui, Y.; Yazaki, Y.; Goto, K.; Masaki, T. *Nature* **1988**, 332, 411.

2. Wu, C. *Exp. Opin. Ther. Pat.* **2000**, *10*, 1653, and references cited therein.
3. Ishizuka, N.; Matsumura, K.; Sakai, K.; Fujimoto, M.; Mihara, S.; Yamamori, T. *J. Med. Chem.* **2002**, *45*, 2041.
4. Wouters, J.; Ooms, F. *Curr. Pharm. Des.* **2001**, *7*, 529.
5. Other than the structures shown in Figures 3 and 4, we have elucidated some crystal structures of **2** and its related compounds. These will be reported elsewhere.
6. Burley, S. K.; Petsko, G. A. *Science* **1985**, *229*, 23.
7. Takasuka, M.; Matsumura, K.; Ishizuka, N. *Vib. Spectrosc.* **2000**, *25*, 6379.
8. Johnson, F.; Malhotra, S. K. *J. Am. Chem. Soc.* **1965**, *87*, 5492.
9. Clark, M.; Cramer III, R. D.; Van Opdenbosch, N. *J. Comput. Chem.* **1989**, *10*, 982.
10. Sakurawi, K.; Yasuda, F.; Tozyo, T.; Nakamura, M.; Sato, T.; Kikuchi, J.; Terui, Y.; Ikenishi, Y.; Iwata, T.; Takahashi, K.; Konoike, T.; Mihara, S.; Fujimoto, M. *Chem. Pharm. Bull.* **1996**, *44*, 343.
11. Altomare, A.; Burla, M. C.; Camalli, M.; Cascarano, M.; Giacovazzo, C.; Guagliardi, A.; Polidori, G. *J. Appl. Cryst.* **435**, 27.
12. *teXsan, Crystal Structure Analysis Package*; Molecular Structure Corporation: 1985 and 1992.